Supplementary information

Graphitic content of gas flaring soot

Before the deconvolution, the raw Raman spectra were treated. First, curves were smoothed by reducing the noise generated in the Raman experiments, then a wavelength range were selected, 500 to 2000 cm^{-1}. To facilitate the peak fitting of the first-order soot Raman bands the baseline signal from the titanium substrate was subtracted. Following these initial steps, the Raman spectra were fitted with an error analysis, which employs the Levenberg–Marquardt algorithm. Two orders of peaks have been previously defined (Sadezky et al., 2005). The first order Raman bands vary between different soot nanoparticles due to different chemical compositions and bonding. Second order Raman bands are derived from the first order Raman bands however, they are less pronounced and may not be distinct in some Raman spectra. Table S1 shows the five main peaks encountered in the first order Raman spectrum of soot aerosols. As recommended by Sadezky et al. (Sadezky et al., 2005), all the peaks are fitted with a Lorentzian curve but the peak D3, which is fitted with a Gaussian curve.

Raman spectra of soot have been deconvoluted to understand the ratios of crystallinity, of amorphous carbon, and of disordered carbon. The optimal fit combinations and deconvolution process have been selected according to: frequency of usage in previous literature references, comparison of the values of the peak ratios obtained with other previous studies, validation of the repeatability by comparing the results from spectra of different points on the same sample, analysis of the influence of the location at which the Raman spectrum is recorded, and observation of the Chi squared value of different statistical approaches.

Soot deconvoluted Raman spectrum is shown in Fig. S1. It was obtained by analyzing soot generated from an H6 gas mixture, a burner with a 50 mm diameter, and a gas outlet velocity of

Table S1 Typical peaks in the Raman spectrum of soot aerosols (Sadezky et al., 2005; Ivleva et al., 2007).

Name	Wavelength [cm^{-1}]	Comments	Description	Curve fit
D4	1127 - 1280	Independent of laser wavelength and intensity	Caused by curved PAH layers in graphitic crystallites.	Lorentz
D1	1280 – 1317	Peak center varies according to the excitation wavelength	Main defect in the graphitic planes of soot, along edge planes of graphitic crystallites	Lorentz
D3	1489 - 1545	Does not vary according to the laser wavelength, but to the type of soot	Induced from impurity ions and amorphous carbon mixtures	Gaussian
G	1580 ± 30	Independent of laser wavelength and intensity	Graphitic planer sheet structures in soot consists of sp^2 bonded carbon atoms	Lorentz
D2	1620 ± 30	Dependent on the soot source	Disorder in polycyclic aromatic hydrocarbons (PAH) around the soot boundaries	Lorentz

0.5 m/s. Lorentzian curves have been selected to fit the peaks D4, D1, G, and D2 and a Gaussian curve has been selected to fit the peak D3.

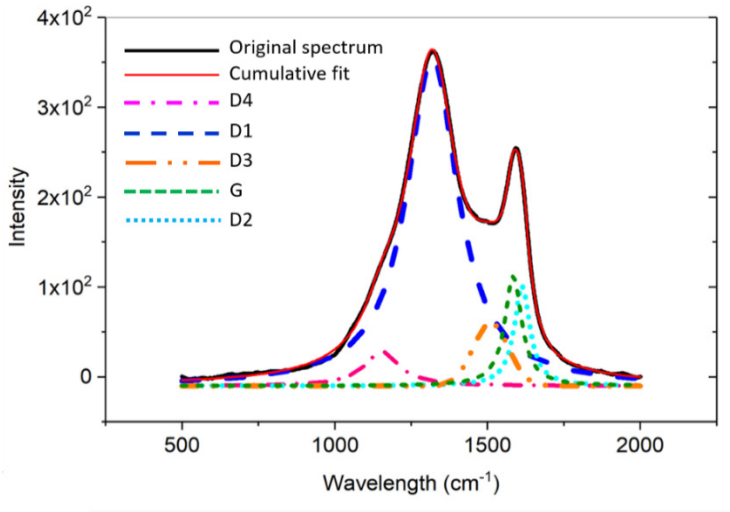

Fig.S1. Soot deconvoluted Raman spectrum of gas flaring soot, indicating five peaks. The example relates to the case of fuel mixture L6, velocity of 0.5 m/s, and burner size of 2".

The relation between the Raman peak ratios and the high heating values of each fuel mixture are shown. Figure S2 shows the correlation between the burner size, at the left-hand side, and the exit velocity, at the right-hand side, with the Raman peak ratios of D1/G and D3/G. No effect of the burner size and the exit velocity is found on the crystallinity of soot aerosols.

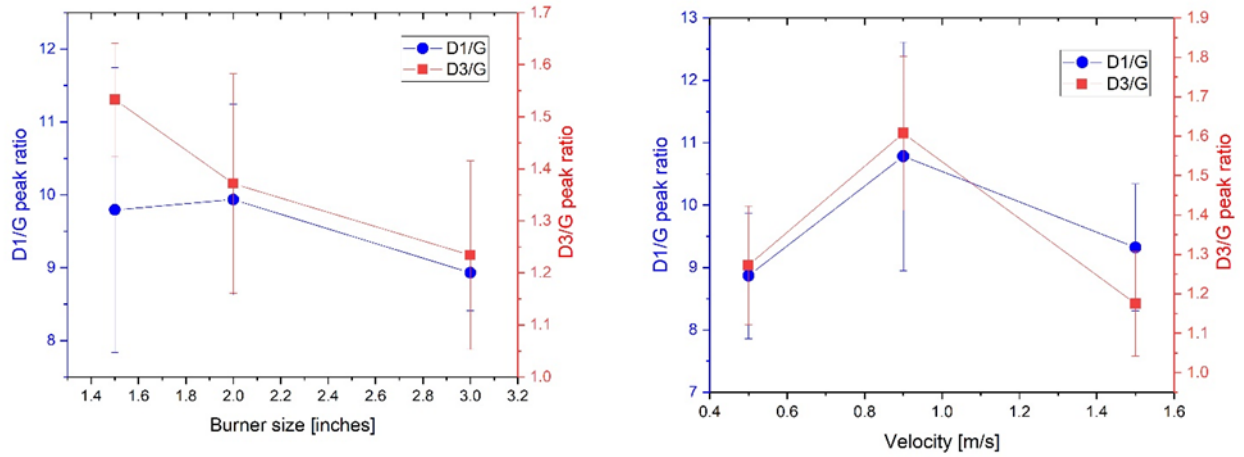

Fig. S2. At the left-hand side, the relationship between the burner size and the D/G peaks is shown. At the right-hand side, the relationship between the velocity and the D/G peaks is shown.

The image processing algorithm does allow for some parameter changes which effect the resulting fringe skeleton. The same default image analysis parameters were used for all images to ensure results could be reliably compared as summarized in Table S2. The thresholding of the image is automatically set using Otsu's method (Otsu, 1979). Regions of Interest (ROIs) were selected based on the guidelines described by (Yehliu et al., 2011).

Table S2. Processing parameters used for the HRTEM image analysis

Processing Parameter	Default Value
Gaussian low pass filter	25 (pixels)
Gaussian low pass filter deviation	2 (1/pixels)
Top-hat transformation disk radius	11 (pixels)
Morphological opening	4 ($pixel^2$)
Morphological closing	4 ($pixel^2$)
Remove small fringes	14 (pixels)

References

Ivleva, N., McKeon, U., Niessner, R. and Pöschl, U. (2007). Raman Microspectroscopic Analysis of Size-Resolved Atmospheric Aerosol Particle Samples Collected with an Elpi: Soot, Humic-Like Substances, and Inorganic Compounds. *Aerosol Science and Technology* 41: 655-671.

Otsu, N. (1979). A Threshold Selection Method from Gray-Level Histograms. *IEEE transactions on systems, man, and cybernetics* 9: 62-66.

Sadezky, A., Muckenhuber, H., Grothe, H., Niessner, R. and Pöschl, U. (2005). Raman Microspectroscopy of Soot and Related Carbonaceous Materials: Spectral Analysis and Structural Information. *Carbon* 43: 1731-1742.

Yehliu, K., Vander Wal, R.L. and Boehman, A.L. (2011). Development of an Hrtem Image Analysis Method to Quantify Carbon Nanostructure. *Combustion and Flame* 158: 1837-1851.